Earth, Planets and Space

FULL PAPER Open Access

Three-dimensional topographic relief of the oceanic crust may control the occurrence of shallow very-low-frequency earthquakes in the Nankai Trough off Kumano

Kazuya Shiraishi[1*], Yasuhiro Yamada[1], Masaru Nakano[1], Masataka Kinoshita[2] and Gaku Kimura[3]

Abstract

To explore a local relationship between geological structures and the occurrence of very-low-frequency earthquakes (VLFEs), a particular class of slow earthquakes with characteristic periods of 10–100 s, we investigated three-dimensional (3D) structural features using reprocessed 3D seismic data from the Nankai Trough off Kumano, southwestern Japan. In this region, VLFEs have been observed along the subducting Philippine Sea Plate. Although the detailed source distribution of VLFEs was estimated by means of recent land-based and offshore seismic networks, the relation with geological features is not well understood. First, we reprocessed the 3D seismic data with advanced techniques and reinterpreted the fault distribution in the sediment layer of the accretionary prism and tracked two key horizons: a décollement and the oceanic crust surface. In the accretionary prism sediments, multiple continuous reflectors of basal detachments in the underthrust sequence and conjugate faults cutting the shallow imbricated thrust sequence were identified. In contrast to the gentle variation in the décollement surface, the topographic relief of the oceanic crust was prominent, with ridges and surface displacement due to faults in the oceanic crust. Then, we compared the structural features with the VLFE source locations. Most VLFEs were located deep in the underthrust sediments where the sediments may consist of underconsolidated muds. Furthermore, a high spatial correlation was observed between the VLFE distribution and the oceanic crust topographic relief. The maximum stress direction, which was inferred from the conjugate faults in the imbricated thrust zone, was consistent with the spatial relation between the VLFE localization and the oceanic crust central ridge. Oceanic crust ridges may cause strain accumulation in the underthrust sediments on the landward sides of the ridges, and low-angle slow thrust movements might be caused using weak slip planes in the underthrust muddy sediments. That is, the topographic relief of the oceanic crust may control the occurrence of shallow VLFEs in the Nankai Trough.

Keywords: 3D seismic images, Very-low-frequency earthquakes, Nankai Trough, Décollement, Oceanic crust, Topographic relief, Conjugate faults

Introduction

Recent observations using land-based and offshore seismic and geodetic networks have revealed spatial variations in the occurrence of slow earthquakes, which are seismic activities with intermediate type of fault slip that is transitional between the fast rupture of regular earthquakes and stable sliding along a megathrust fault interface (Obara and Kato 2016). Slow earthquakes are typically classified as slow-slip events (SSEs) with durations of days to years, very-low-frequency events (VLFEs) with periods of 10–100 s, impulsive low-frequency earthquakes (LFEs) with frequencies around several hertz,

*Correspondence: kshiraishi@jamstec.go.jp
[1] Japan Agency for Marine-Earth Science and Technology, 3173-25, Showa-machi, Kanazawa-ku, Yokohama, Kanagawa 236-0001, Japan
Full list of author information is available at the end of the article

and low-frequency tremor (LFT), and their occurrence times and locations are correlated (e.g., Ito et al. 2007). Many investigations have been conducted to explore the mechanism of slow earthquakes and their connection with large earthquakes. Various types of slow earthquakes have been observed in plate subduction zones around the world: Cascadia (Rogers and Dragert 2003), Mexico (Kostoglodov et al. 2003), New Zealand (Wallace and Beavan 2010; Wallace et al. 2016), and Japan (Ito et al. 2007; Yamashita et al. 2015; Nishikawa et al. 2019). In the Nankai Trough, southwestern Japan, Ito and Obara (2006) detected VLFEs using a land-based seismic network. In the same region, Obana and Kodaira (2009) and Sugioka et al. (2012) detected LFTs and VLFEs, respectively, using long-term ocean bottom seismic observations. Araki et al. (2017) detected shallow SSEs in the Nankai trough using subseafloor borehole observatories with pressure gauges and revealed that the SSEs occurred repeatedly and that some of them were triggered by other earthquakes. Nakano et al. (2018) located the sources of VLFEs with a dense ocean bottom seismic network and revealed the spatial localization and temporal migration of VLFE occurrences in a 1-month period in April 2016. Takemura et al. (2019) also located VLFE sources from observations using the land-based seismic network of southwestern Japan in a wide area along the Nankai Trough during a long interval from 2016 to 2018. These studies suggest spatial variations in the distribution and their mechanism along the subducting Philippine Sea Plate boundary (Obara and Kato 2016).

To understand the spatial variations in slow earthquake occurrence, the effect of geological structures is an important factor to investigate in detail. On the northern Hikurangi margin, which is one of the well-studied areas, seamount subduction has been suggested to influence the mechanism of SSEs, including the effects of the stress state and fluid migration in the deformed upper plate (Todd et al. 2018; Shaddox and Schwartz 2019; Sun et al. 2020). In the Nankai Trough, Ito and Obara (2006) and Obana and Kodaira (2009) discussed the possibility of dynamic deformation by reverse faults within the accretionary prism. Sugioka et al. (2012) suggested that the décollement of the imbricated thrust zone was a favorable slip plane for VLFEs. Toh et al. (2018) investigated the effect of large subducting ridges imaged by two-dimensional (2D) seismic data in the Tonankai region (Park et al. 2003) on VLFE occurrence. Tonegawa et al. (2018) reported that VLFEs were activated in areas with sporadic distributions of low S-wave velocity bodies beneath seismic stations along the Nankai Trough. Kitajima and Saffer (2012) and Tsuji et al. (2014) noted that the underlying sedimentary sequence of the imbricated thrust zone in the accretionary prism was a potential area for VLFE occurrence based on their quantitative estimation of possible high pore pressure. Seismic data can provide high-resolution structural features, which are useful to compare the local effects on shallow VLFE activities. The spatial characteristics of VLFE occurrence, however, have not been well studied based on 3D high-resolution geological structures.

To further understand the local VLFE occurrence in the Nankai Trough accretionary prism, high-resolution information on the geological structure should be extracted from 3D seismic data. In our study, we investigated the structural features from newly reprocessed 3D seismic images from an offshore area of Kumano where VLFEs have been repeatedly observed. The 3D seismic data were acquired in 2006 (Moore et al. 2007) and reprocessed in 2016 to better understand the seismogenic zones (Shiraishi et al. 2019a). Since many VLFEs in and around the seismic survey area are well documented by Nakano et al. (2018), this is one of the best areas to investigate a local relationship between geological structures and VLFE occurrences.

In this paper, we further reprocessed the 3D seismic data in the area of the VLFE occurrences and reinterpreted the fault distribution in the shallow sediments in the accretionary prism, and we tracked two key horizons: a décollement and the oceanic crust surface. We compared the local structure with VLFE source distributions. We discussed the possible local effects of the oceanic crust topographic relief and the related fault distribution on VLFE occurrence in this area.

Geological setting

The Nankai Trough is located southwest of Japan (Fig. 1a), where the Philippine Sea Plate is subducting to the northwest beneath the Amurian Plate at rates of 40–65 mm/year and azimuths of approximately 300°–315° clockwise from the north (Seno et al. 1993; Miyazaki and Heki 2001; Bird 2003). The Shikoku Basin is the northern margin of the subducting Philippine Sea Plate and is filled with thick layers of hemipelagic muds and turbidites. The large volume of sediments has caused the rapid evolution of the accretionary prism throughout the various accretion phases (e.g., Taira 2001; Kimura et al. 2014).

Based on many seismic surveys using 2D and 3D multichannel seismic (MCS) systems and 2D wide-angle seismic surveys using linear arrays of ocean bottom seismographs (e.g., Kodaira et al. 2000; Park et al. 2003; Moore et al. 2007; Nakanishi et al. 2008), the regional crustal structures and fault distributions in this region are generally well known. The accretionary prism can be divided into the outer prism (seaward region) and the inner prism (landward region) around the seaward edge

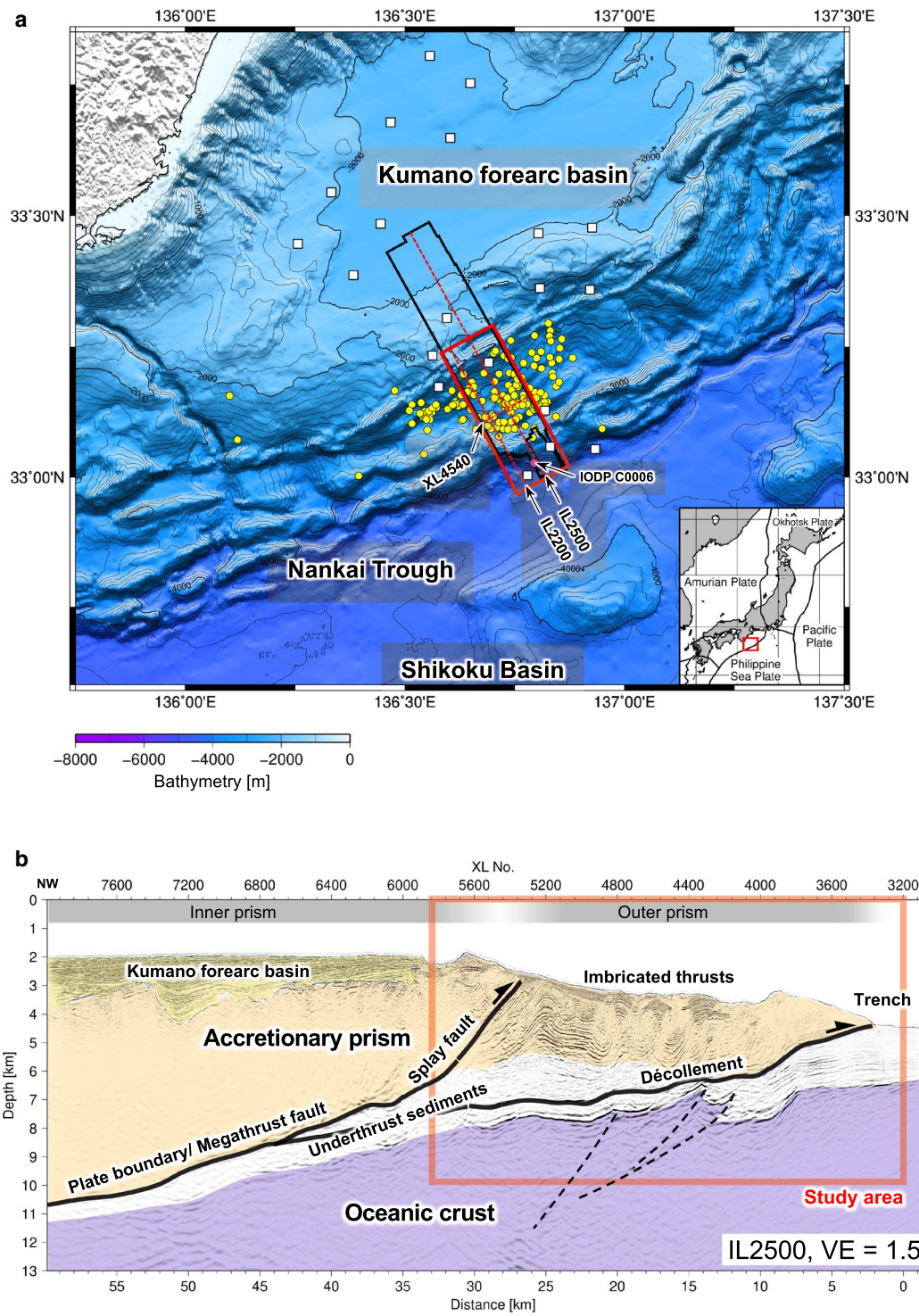

Fig. 1 Overview of the 3D seismic survey area and the distribution of VLFEs in the Nankai Trough. **a** Map of the survey area southeast of the Kii Peninsula, Japan. The black polygon indicates the area of the 3D MCS survey in 2006 (Moore et al. 2007). The red rectangle indicates the target area in this study, and the red dashed lines indicate the locations of vertical sections shown in Figs. 1b and 3. The yellow circles are the epicenters of VLFEs located by Nakano et al. (2018). The white squares denote the locations of ocean bottom seismic stations of the DONET. The magenta circle denotes the location of IODP Site C0006. **b** A vertical section along line IL25000 with vertical exaggeration (VE) of 1.5. The accretionary prism is divided into the inner prism and outer prism by a splay fault. Our study area enclosed by the red rectangle is characterized by imbricated thrusts and an underthrust succession above the oceanic crust

of the Kumano Basin by an out-of-sequence thrust, or a splay fault, branching from the plate interface (Fig. 1b). The splay fault is considered one of the primary coseismic faults of tsunamigenic earthquakes (e.g., Moore et al. 2007). Sakaguchi et al. (2011) also showed evidence of coseismic slip at the updip end of the plate boundary fault and along the décollement at the toe of the accretionary prism, from core samples at the Integrated Ocean Drilling Program (IODP) Site C0006 (Fig. 1a, magenta dot). In addition to historical tsunamigenic earthquakes that have occurred repeatedly with recurrence intervals of 100–200 years (Ando 1975), slow earthquake activity has been identified by recent observations as mentioned above (e.g., Ito and Obara 2006; Obana and Kodaira 2009; Araki et al. 2017; Nakano et al. 2018; Takemura et al. 2019).

In the outer accretionary prism, where shallow VLFEs and LFTs are frequently observed, the spatial and temporal evolution of the splay fault have been documented using 3D seismic data and drilling data (Strasser et al. 2009; Kimura et al. 2011; Yamada et al. 2013). The outer accretionary prism is actively deforming with imbricated thrust faults (Fig. 1b). In contrast to the alternating succession in the overlying sequence with imbricated thrusts, the underlying sequence is less reflective, and it is considered to contain underthrust sediments of massive hemipelagic muds deposited in the Shikoku Basin (e.g., Park et al. 2010; Uunderwood et al. 2010). The possibilities of low velocity (Park et al. 2010; Kamei et al. 2012) and pore-fluid overpressure (Kitajima and Saffer 2012; Tsuji et al. 2014) in the underthrust sediments have been suggested. Within the underthrust sediments, a clear positive reflection surface marking a décollement is recognized, which continues from the deep plate boundary megathrust fault to the trench (Fig. 1b).

Data and methods

Reprocessed 3D MCS PSDM images

To analyze the 3D structures, we used 3D seismic data that were acquired in a southeastern offshore area off the Kii Peninsula in 2006 (Fig. 1, black polygon) (Moore et al. 2007). Two airgun arrays with a 75 m spacing, each totaling 50.64 L (3090 cubic inches) with 13.8 MPa (2000 psi), were alternately fired at 37.5 m shot intervals. Four 4.5-km hydrophone streamer cables with 360 receiver groups at a 12.5 m spacing were towed 150 m apart. The resulting 3D dataset covered an area of approximately 62.5 km × 12 km with irregular boundaries around the trench because of acquisition difficulties due to the high-speed Kuroshio current. The initial preprocessing and a full 3D prestack depth migration (PSDM) were performed in 2006 (Moore et al. 2009). The 3D bins for the final migrated data were located every 12.5 m in the inline direction (NW–SE) and every 18.75 m in the crossline direction (SW–NE).

Based on the improved results from the reprocessing of the middle part from XL 4750 to XL 6750 in 2016 (Shiraishi et al. 2019a), we additionally applied the same methods to the southern part from XL 3000 to XL 4750 in 2018. We seamlessly merged the two reprocessed volumes of the neighboring parts to one volume. The preprocessing from the original data included an optimal combination of several methods to attenuate noise and multiple reflections, broadband processing with deghosting to recover desirable frequency responses, and data regularization to mitigate nonuniform fold distribution. Using the preprocessed data, a P-wave velocity model for PSDM and the PSDM volumes of both Kirchhoff migration (e.g., Sheriff 2002) and beam migrations (Sherwood et al. 2009) were produced (see details in Shiraishi et al. 2019a). The image quality of the new PSDM results was better than that of the legacy PSDM result (Fig. 2). The images from the Kirchhoff PSDM (Fig. 2b, e) were useful for interpreting the detailed deformation structures in the accretionary prism (Shiraishi et al. 2019a, b). The beam PSDM images (Fig. 2c, f) with better continuity and less noise than in the Kirchhoff PSDM images were useful for interpreting deeper parts (Shiraishi et al. 2019a). In this study, we focused on the southern part XL 3200–5800 of the 3D survey box where VLFEs occurred (Fig. 1a, b, red rectangles) and the southern end of the study area was limited because of poor images in the southernmost area due to irregular boundary of data acquisition. The extracted vertical sections of the beam PSDM in the NW–SE direction in our study area are shown in Fig. 3.

Structural interpretation by horizon picking and seismic attributes

To investigate the structural features, we interpreted horizons (i.e., stratigraphic surfaces) with the reprocessed 3D PSDM images. We tracked two horizons, i.e., a décollement and the top of the oceanic crust, by manually picking their reflections on the seismic sections at every 5 or 10 lines in the NW–SE direction and smoothly interpolating them for each continuous surface. The surfaces divided by displacement due to faults were treated separately, as shown in Fig. 4.

To analyze the fault distribution in shallow sediments, we generated a semblance-based coherence cube (Marfurt et al. 1998) from the Kirchhoff PSDM volume. The coherence is a measure of similarity among surrounding traces (e.g., Sheriff 2002) such that higher values indicate more continuous reflection events and lower values indicate more discontinuities, such as layer boundaries or faults. The common depth slices extracted from the

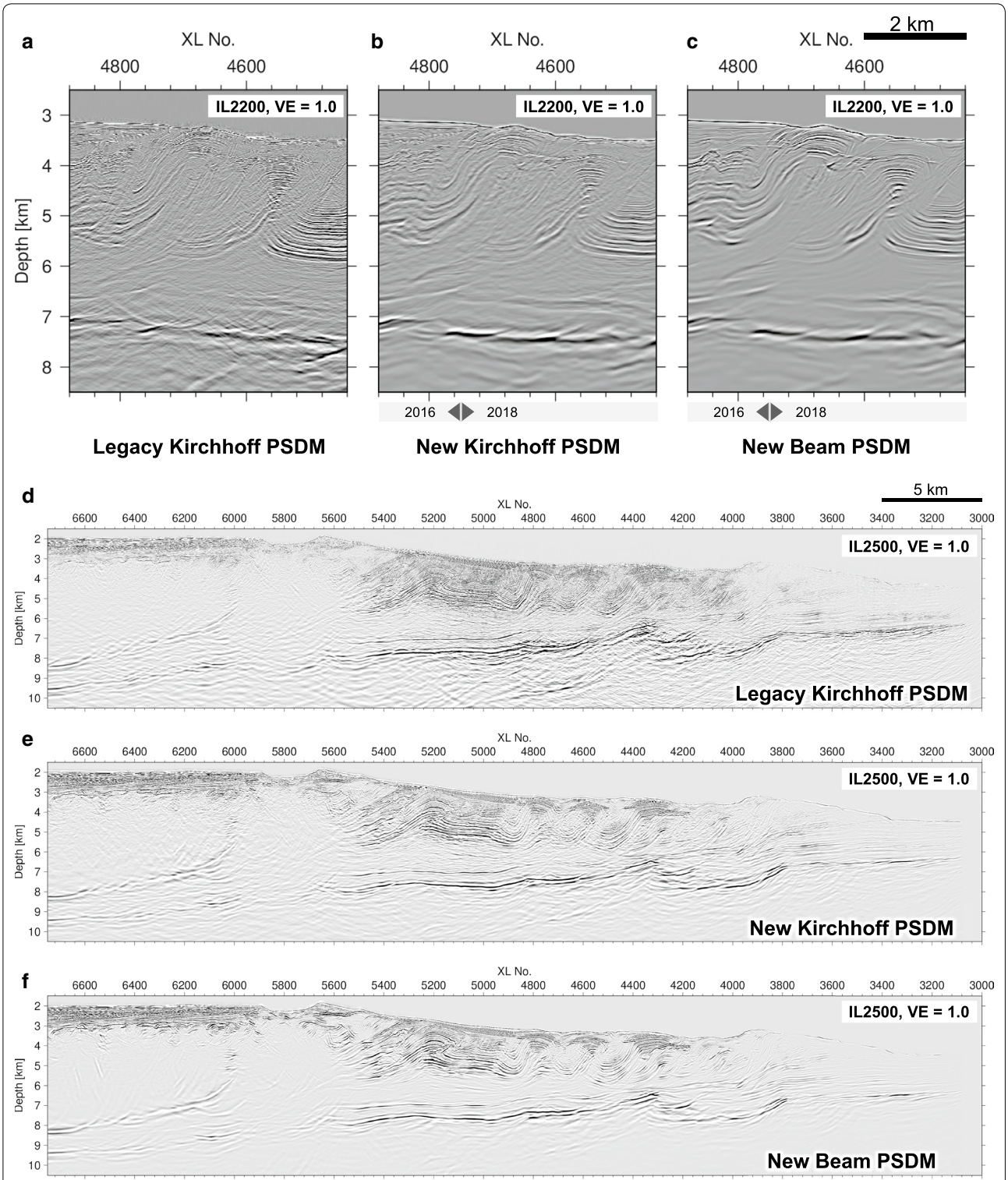

Fig. 2 Comparison of enlarged vertical sections extracted from 3D PSDM volumes along IL 2200: **a** legacy Kirchhoff PSDM in 2006, **b** new Kirchhoff PSDM in 2016–2018 and **c** new beam PSDM in 2016–2018. Comparison of vertical sections of the whole reprocessed range along IL 2500: **d** legacy Kirchhoff PSDM, **e** new Kirchhoff PSDM and **f** new beam PSDM. Vertical exaggeration is 1.0

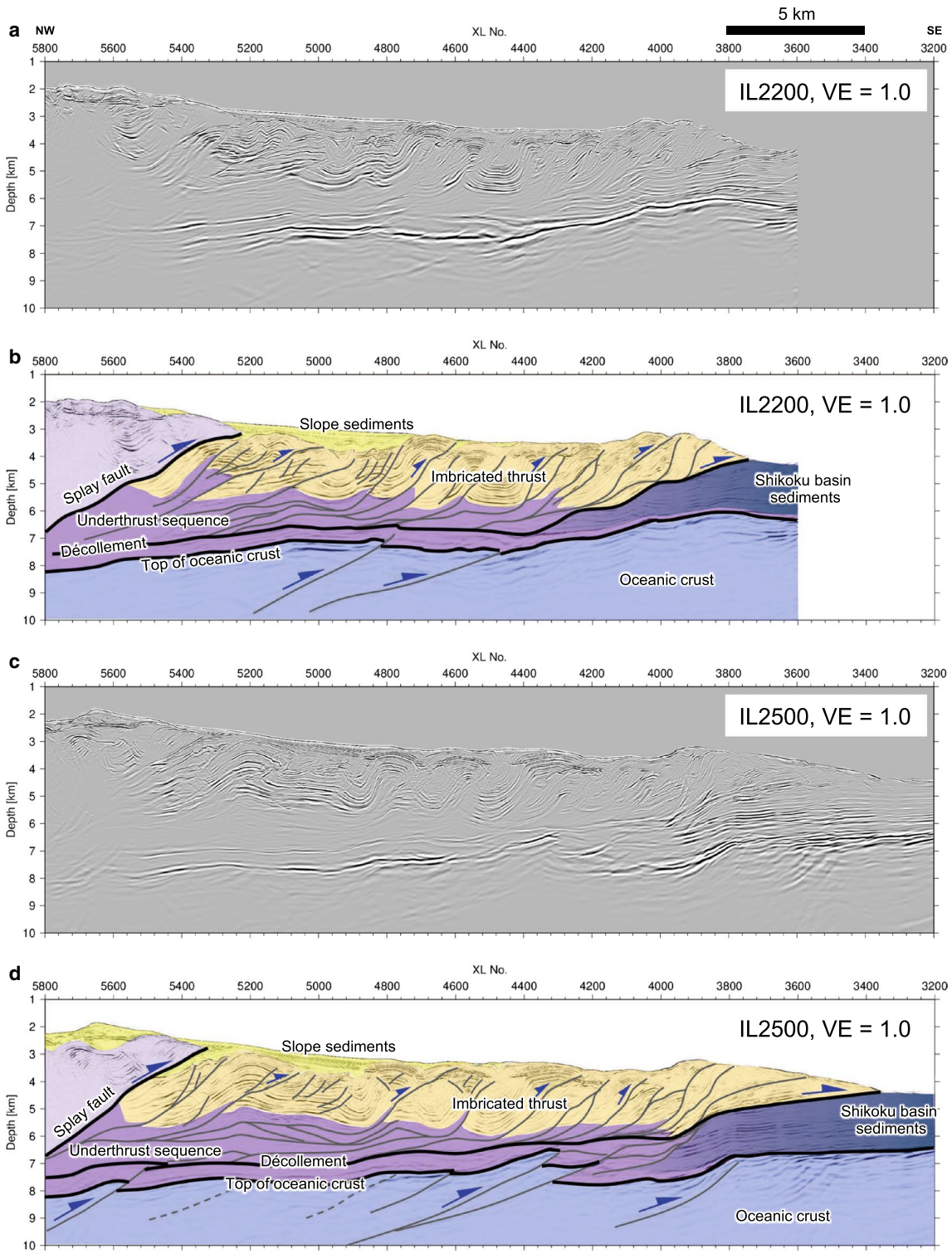

Fig. 3 Vertical sections extracted from a 3D beam PSDM volume along the NW–SE direction. **a** Seismic section along IL 2200 and **b** structural interpretation of (**a**). **c** Seismic section along IL 2500, and **d** structural interpretation of (**c**). Vertical exaggeration (VE) is 1.0 for all sections in this figure

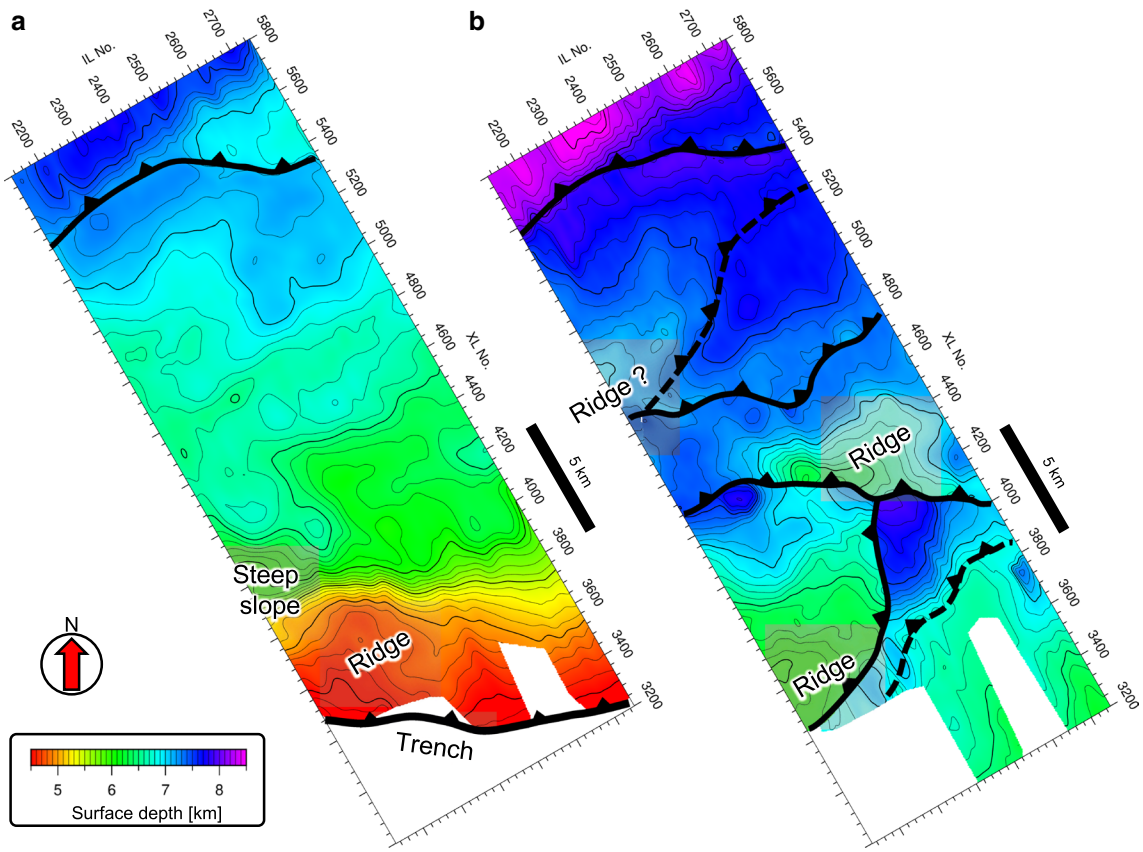

Fig. 4 Interpreted horizons of (**a**) the décollement and (**b**) the top of the oceanic crust. The black lines with triangles denote faults (and trench in (**a**)). The décollement is generally a gently sloping surface and has a locally steep slope in the SW area. The top of the oceanic crust has prominent topographic relief due to faults in the oceanic crust, and there are ridges on the surface

coherence cube were used to interpret the horizontal fault distribution (Fig. 5).

VLFE source distributions

To compare the obtained structural features with VLFE occurrence, we used an existing VLFE source catalog obtained by Nakano et al. (2018) (Fig. 1, yellow dots) in which the centroid moment tensors (CMTs) of VLFEs that occurred in April 2016 were obtained by waveform inversion using data from a permanent ocean bottom seismic network, the Dense Oceanfloor Network system for Earthquakes and Tsunamis (DONET; Kaneda et al. 2015; Kawaguchi et al. 2015). Figure 6a shows the epicenter distribution. The VLFEs were distributed in the outer prism parallel to the trough axis. Figure 6b shows the standard errors of the source locations in two horizontal directions and the depth direction estimated by bootstrapping (Nakano et al. 2018). The average location errors were 0.0424° (approximately 3.95 km) and 0.0383° (approximately 4.26 km) in longitude and latitude, respectively, and 1.62 km in depth.

In our study, we used only the VLFE sources located with higher accuracy and having standard errors smaller than the average values in each direction described above. The resultant sources can be separated into several clusters (Fig. 6c). We successfully removed misaligned events located outside the observation network or small events for which few waveforms were available. Figure 6d shows a comparison of the source depth distributions before and after the screening, which ensures that the locations of deeper events that are less accurate have been removed. The selected events are mostly located between depths of 5.5 km and 7.5 km. We note that the source locations of Nakano et al. (2018) are based on the 1D velocity structure of P- and S-waves in this region, and systematic errors of a few km deep or landward may exist because of the heterogeneous structure in the horizontal directions in the accretionary prism.

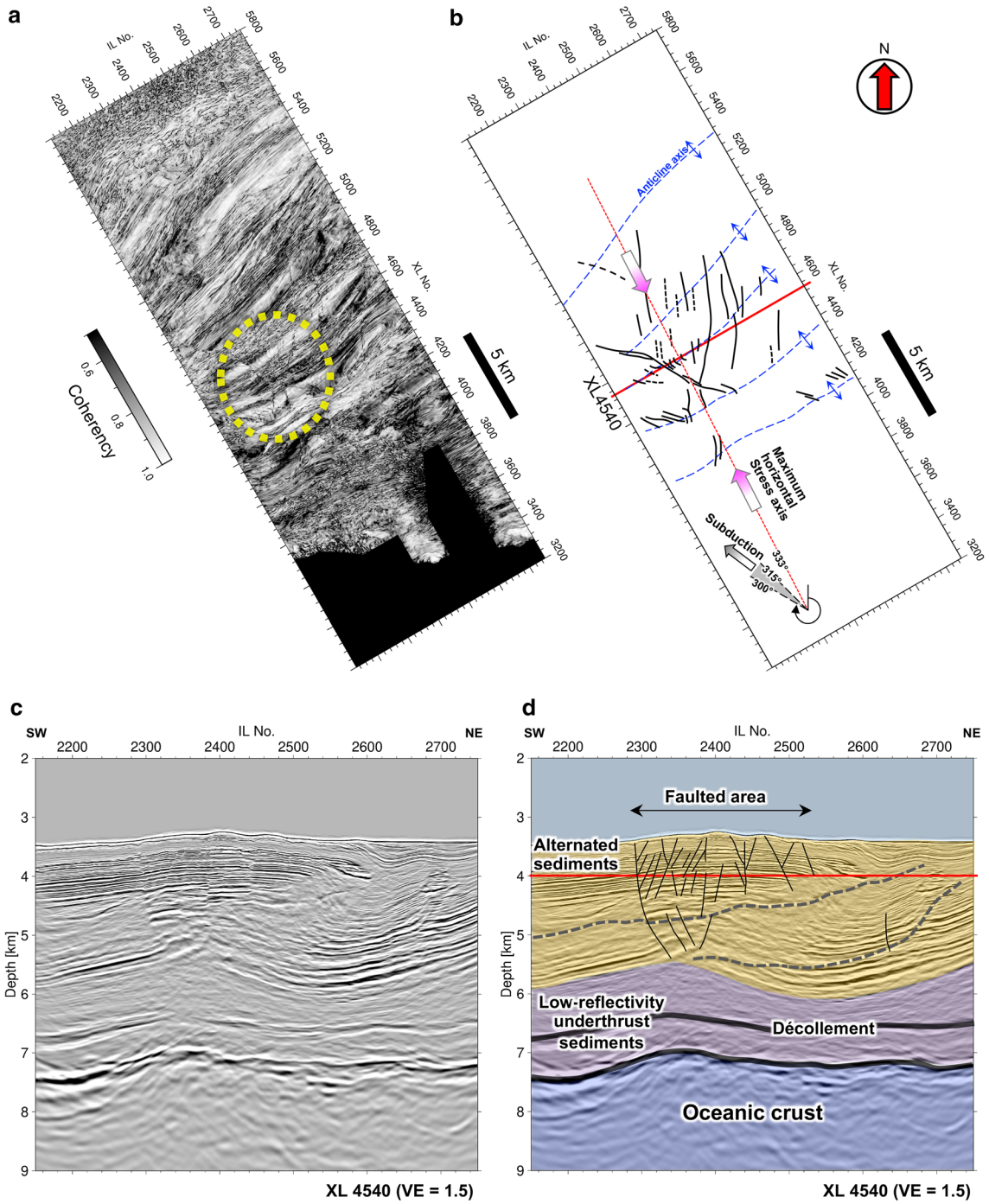

Fig. 5 Fault distribution in the shallow sediments. **a** A horizontal slice of the coherence cube at a depth of 4 km. Conjugate faults cutting the in-sequence thrusts are identified in the area with the yellow dashed circle. **b** The interpreted fault distributions identified on the horizontal slice are shown with black lines. The blue dashed lines indicate the anticlinal axes of folds in the imbricated thrust zone. The maximum horizontal axis inferred from the horizontal fault distribution is approximately 333° clockwise from the north, which is oblique to the subduction direction 300°–315°. **c** Vertical sections along the SW–NE direction (XL 4540) of the Kirchhoff PSDM image and **d** the same image as (**c**) with structural interpretation. The vertical displacements and topographic variations in the seafloor can be interpreted in the faulted area due to subsequent faults

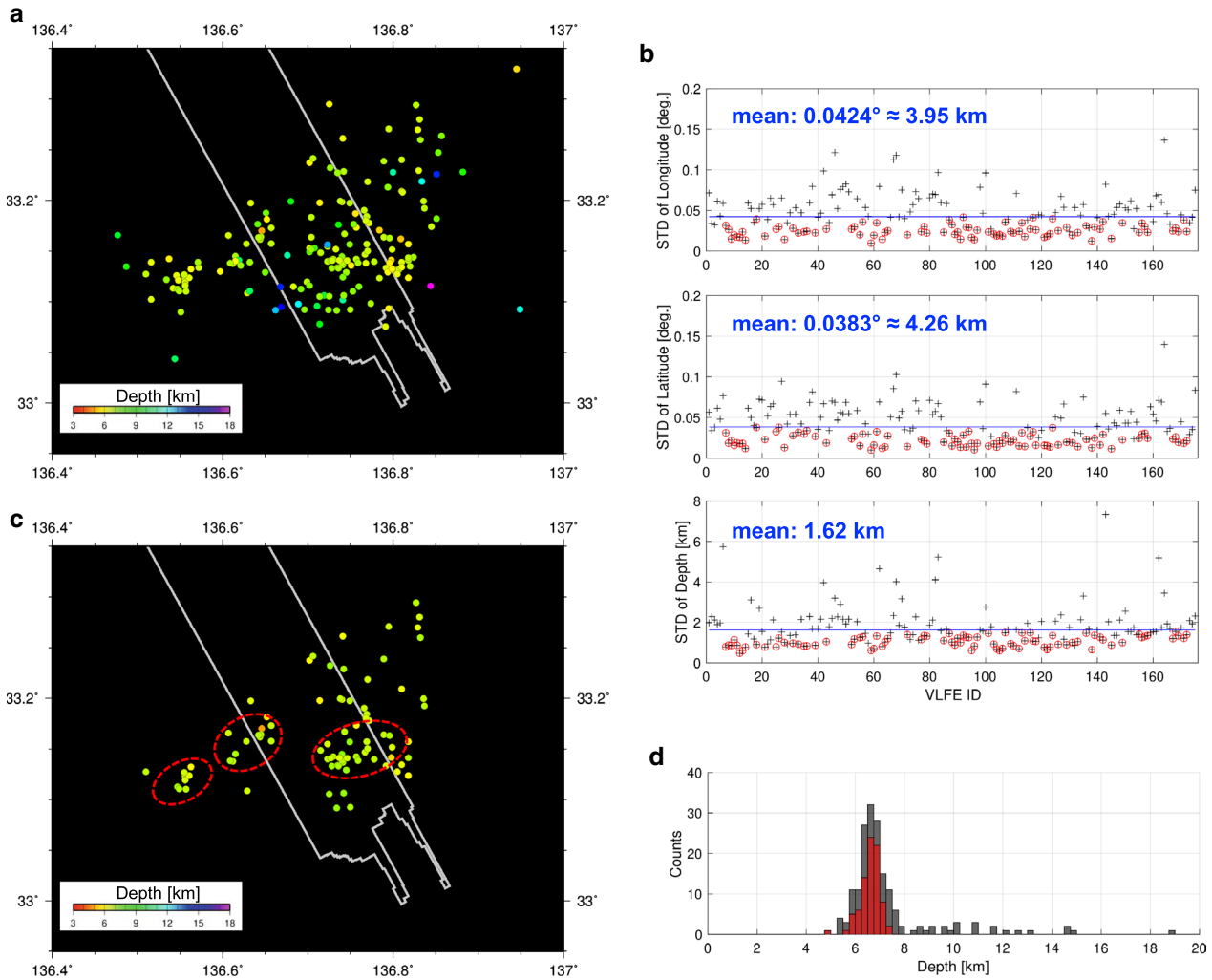

Fig. 6 **a** Distribution of VLFE sources (Nakano et al. 2018). **b** Standard errors of the VLFE source locations in the longitude, latitude, and depth directions (black crosses). The red circles indicate VLFE sources whose errors are lower than the mean value of the standard deviation (STD) for each direction. **c** The distribution of VLFEs with location errors smaller than the mean value of the STD; the red dashed circles indicate VLFE clusters. **d** Histograms of the depth distribution of the original (gray) and selected (red) VLFEs

Results

A complex thrust fault distribution is observed in the accretionary prism (Fig. 3). In contrast to the alternating sediments in the overlying imbricated thrust sequence, the thick underlying sequence is less reflective above the oceanic crust. A clear reflector within the low-reflectivity sequence has been considered a décollement (e.g., Moore et al. 2007). In the reprocessed images, several continuous reflectors are clearly identified in the thick low-reflectivity sequence above the décollement. Some of these reflectors can be traced as detachments that are continuous from shallow thrust faults to the décollement (Fig. 3b, d).

The two interpreted horizons, the décollement and the top of the oceanic crust, generally deepen from southeast to northwest (Fig. 4). The slope of the décollement surface is mostly gentle but partly steep in the southwestern area and approximately 6 km landward from the trench (Fig. 4a). Regarding the top of the oceanic crust (Fig. 4b), topographic relief is prominent with several ridges and faults. The topographic relief is caused by faults in the oceanic crust, which are part of the widely distributed thrust and strike-slip faults in this region and have grown in the oceanic crust before and during plate subduction in regional tectonics (Tsuji et al. 2009, 2013). A remarkable ridge in the oceanic crust surface with a topographic

height of approximately 1 km and an area of approximately 3 km × 8 km is present in the central part near IL2400–2500 and XL 4400 (Fig. 4b). The topographic change in the décollement above the central ridge in the oceanic crust is small, while the topographic high associated with the steep slope of the décollement in the southwestern area corresponds to another ridge in the oceanic crust.

In the horizontal slice of the coherence cube at a depth of 4 km from mean sea level (Fig. 5a, b), the typical features of imbricated fold-and-thrust structures and conjugate strike-slip faults cutting the in-sequence thrusts are identified (Fig. 5a). The vertical displacement of the conjugate faults and related faults can be observed in the SW-NE vertical sections (Fig. 5c, d). The conjugate faults on the horizontal slice imply the principal stress direction, which can be inferred as approximately 333°. The inferred principal stress direction is approximately perpendicular to the anticline axes and oblique to the direction of Philippine Sea Plate subduction at 300°–315° (Fig. 5b).

Projecting the selected VLFE sources on a vertical section extracted from the 3D PSDM volume, most of the VLFEs are located in the low-reflectivity sequence between the shallow imbricated thrust sequence and the oceanic crust (Fig. 7a). On the plane view of the oceanic crust surface with the VLFEs, a localized distribution of VLFE sources can be recognized in the area approximately 4 km northwest of the central ridge of the oceanic crust (Fig. 7b). The conjugate faults are located in the area approximately 5 km northwest of the steep slope of the décollement (Fig. 7c), while the fault distribution does not correspond to the VLFE sources and oceanic crust topography. The spatial relation between the central ridges and VLFEs is consistent with the direction of the maximum horizontal stress inferred from the conjugate faults rather than the direction of plate subduction (Fig. 7b). The slip directions of low-angle reverse fault movements from the CMT solutions of VLFEs are also consistent with the direction of the present maximum horizontal stress (Fig. 7a, b).

Discussion

Detachments in the underthrust sequence

We identified some novel continuous reflectors in the thick low-reflectivity sequence that may be part of the detachment of the thrust faults likely converging to the décollement. In terms of the low-reflectivity sequence, Park et al. (2010) and Kamei et al. (2012) noted that the seismic velocity in the underlying low-reflectivity sequence was lower than that in the overlying imbricated thrust sequence by analyzing the 3D MCS data and 2D wide-angle seismic data acquired with ocean bottom seismographs. The thick low-reflectivity sequence was inferred to represent underthrust sediments with currently forming antiformal stacking (Park et al. 2010; Tsuji et al. 2014). The underthrust sediments consist of hemipelagic muds accompanied by turbidites and volcanic ash that were deposited in the Shikoku Basin before subduction (e.g., Park et al. 2010; Uunderwood et al. 2010). The underthrust mud-dominant sediments are considered underconsolidated (Bangs et al. 2009; Park et al. 2010) and have high pore pressure (Kitajima and Saffer 2012; Tsuji et al. 2014).

The clear continuous reflectors in the underthrust sediments may be detachments of the in-sequence thrust faults that might have developed using thin weak layers within the massive underconsolidated muddy sediments. Tsuji et al. (2014) noted that discontinuous reflections above the décollement imply structures deformed by shear zones within the underthrust sequence. These continuous and discontinuous detachments might work as slip planes in addition to the major décollement in the underthrust sediments.

Stress field inferred from the conjugate faults cutting in-sequence thrusts

We identified the conjugate faults in the shallow imbricated thrust sequence and inferred that the maximum horizontal stress axis is oriented 333°. The inferred stress direction is almost consistent with the maximum stress direction of 330°, which was estimated from borehole breakout analyses at Site C0006 (Fig. 1, magenta dot) (Lin et al. 2016). This consistency in the maximum stress direction, which is oblique to the direction of plate subduction, implies that conjugate faults were generated in the present stress field within the accretionary prism. Furthermore, the conjugate faults with vertical displacements subsequently cutting the in-sequence thrust faults (Fig. 5) imply a possible change in the stress field from a reverse fault regime to a strike-slip fault regime with upward movement.

The conjugate faults are located in the area northwest of the topographic high of the décollement and their positional relationship is in the same direction as the maximum horizontal stress axis (Figs. 5d and 7c). This relationship suggests that a possible change in the stress regime was caused by the steeper slope of the décollement around the southwest area. Wang and Bilek (2011, 2016) reviewed the mechanism of seamount subduction and explained that geometric incompatibility must be overcome by the deformation of the surrounding rocks and the seamount itself with a complex network of fractures. A 3D numerical simulation study by Ruh et al. (2016) suggested that uplift movement with tectonic underpressure may generate extension in the shallow

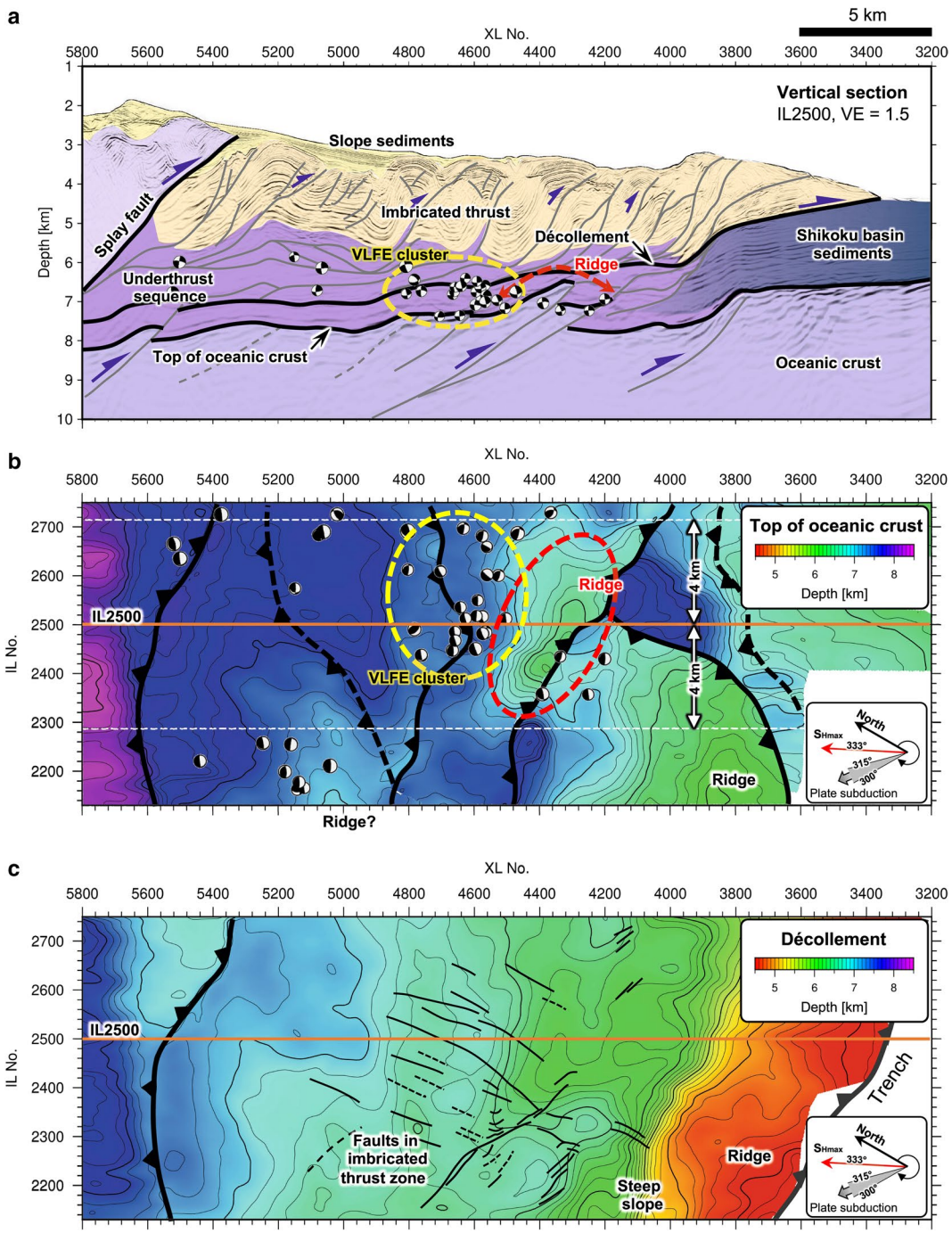

Fig. 7 Comparisons of the 3D seismic images, structural features, and VLFE source distributions. **a** CMT solutions within 4 km, approximately the maximum spatial error, from line IL2500 are projected on the seismic section. The vertical exaggeration (VE) of the seismic section is 1.5. Most of the selected VLFEs are located in low-reflectivity underthrust sediments on the landward side of the central ridge in the oceanic crust and are thought to consist of underconsolidated hemipelagic muds. **b** The oceanic crust topography and VLFE distribution with the CMT solutions. A cluster of VLFEs is located on the landward side of the central ridge in the oceanic crust. **c** The décollement topography and fault distribution in the shallow imbricated thrust sequence. The conjugate faults are also located on the landward side of the topographic high of the décollement. These comparisons imply that the maximum stress direction, which is inferred from the conjugate faults in the imbricated thrust zone, is consistent with the slip direction of VLFEs and the spatial relation between the VLFE distribution and the oceanic crust ridge. The consistencies suggest that the activity and distribution of VLFEs are controlled by the relief of the oceanic crust affecting the present stress field in the overlying sequence

part of the rear side of an underthrusting seamount. Accordingly, conjugate faults with vertical displacements on the landward side of the steeper décollement may be generated in a manner similar to that of the stress field on the rear side of an underthrusting seamount.

3D structural features and VLFE occurrence

A spatial comparison between the structural features and the VLFE source (Fig. 7) implies a high correlation of the VLFE occurrence with the central ridge in the oceanic crust topographic relief rather than with the décollement surface. Most of the VLFEs are located in the thick underthrust sequence at depths of 5.5–7.5 km (Fig. 7a), where the major décollement and other possible detachments may work as potential slip planes in the underthrust sediments. The VLFE sources in a cluster (Fig. 6c) are localized 3–4 km northwest of the central ridge in the oceanic crust (around XL4400–4800 in Fig. 7a). Both the slip directions of VLFEs and the spatial relation between the ridges and VLFEs are consistent with the direction of the maximum horizontal stress rather than the direction of plate subduction (Fig. 7a, b). These consistencies suggest that the activity and distribution of VLFEs are governed by the subducting ridges in the oceanic crust and the present stress state in the overlying sequence. In the area above the relatively flat surface of the oceanic crust on the landward side of the central ridge, seismic activity potentially occurs due to local compressive stress accumulation caused by the ridge with a topographic height of approximately 1 km (Fig. 7a, b). The 3D numerical simulation by Ruh et al. (2016) showed that tectonic overpressure (stress accumulation) was generated on the rear side (landward side) along the flank of a subducting seamount. Indeed, earthquakes with possible stress accumulation have been observed on the landward sides of seamounts (e.g., Mochizuki et al. 2008; Geersen et al. 2015). The mechanism of SSEs and tremors in the northern Hikurangi margin is influenced by subducted seamounts (e.g., Wallace et al. 2016; Todd et al. 2018; Shaddox and Schwartz 2019). In a similar manner, the VLFEs may occur due to local stress accumulation in the underthrust sediments caused by underthrusting ridges in the oceanic crust in our study area. The topographic relief with ridges and faults in the subducting oceanic crust may affect the local VLFE distribution in addition to subducting seamounts that affect the regional seismic activity.

Consequently, we propose that the topographic relief of the oceanic crust is an important factor controlling the occurrence of VLFEs. Most of the VLFEs, which were observed as low-angle thrust movements in April 2016 (Nakano et al. 2018) (Fig. 7a), may occur along the décollement or neighboring detachments in the underthrust muddy sediments under the condition of overpressure around the landward side of the oceanic crust ridges. We note that the source locations estimated with the 1D velocity structure may contain possible systematic errors in depth or landward position because of the heterogeneous structure in the accretionary prism. To reduce errors in estimating VLFE source locations, realistic 3D velocity models of both P- and S-waves and efficient modeling methods dealing with heterogeneous models are necessary in addition to improved dense and wide observations by offshore seismic networks. To further understand the mechanism of VLFEs and other seismic activity with respect to geological structures in the wide area of the Nankai Trough, detailed investigations with dense seismic surveys are required to characterize the oceanic crust topography and overlying sediments.

Conclusions

We showed a local relationship between 3D structures and shallow VLFEs in the Nankai Trough off Kumano. We identified new structural features based on the reinterpretation of the 3D seismic data and compared them with the reliable source locations of VLFEs.

1. VLFEs with low-angle thrust movements may occur along detachments in the underthrust sediments. The topographic relief of the oceanic crust and slip planes in the overpressured sediments on the landward sides of the oceanic crust ridges may control the occurrences of the shallow VLFEs in the Nankai Trough.
2. Multiple detachments of imbricated thrusts, which may provide potential slip planes in the low-reflectivity underthrust sediments, were identified above the décollement. In contrast to the gentle topography of the décollement, the topographic relief of the oceanic crust is prominent. Newly identified conjugate faults cutting the shallow in-sequence thrusts with vertical displacements imply that the maximum horizontal stress direction is oblique to the direction of plate subduction.
3. Most of the VLFEs are located in the deep underthrust sediments, which consist of massive underconsolidated muds, possibly with high pore pressure. The localized VLFE sources are found northwest of the oceanic crust ridges, and the spatial relationship between them is consistent with the direction of the maximum stress. The underthrusting ridges in the oceanic crust may affect the stress accumulation in the underthrust sediments.

Abbreviations
VLFE: Very-low-frequency earthquake; LFE: Low-frequency earthquake; LFT: Low-frequency tremor; SSE: Slow slip event; MCS: Multichannel seismic; PSDM: Prestack depth migration; CMT: Centroid moment tensor; DONET: Dense Oceanfloor Network system for Earthquakes and Tsunamis; IODP: Integrated Ocean Drilling Program (presently, International Ocean Discovery Program).

Acknowledgements
This work was supported by the Japan Society for the Promotion of Science (JSPS) KAKENHI Grant-in-Aid for Scientific Research S (JP15H05717). We thank two anonymous reviewers and the editor for providing comments that improved the manuscript.

Authors' contributions
KS interpreted geological structures and their relationship with the VLFE distribution and drafted the manuscript. YY discussed geological structures and modified the manuscript. MN discussed the VLFE source distribution and modified the manuscript. MK and GK supervised the 3D data reprocessing project and provided helpful comments. All authors read and approved the final manuscript.

Funding
Japan Society for the Promotion of Science (JSPS) KAKENHI Grant-in-Aid for Scientific Research S (JP15H05717); Management expense grants at the Japan Agency for Marine-Earth Science and Technology (JAMSTEC).

Availability of data and materials
The reprocessed 3D PSDM volumes are available from the JAMSTEC data catalog (http://www.godac.jamstec.go.jp/catalog/data_catalog/e/index.html).

Ethics approval and consent to participate
Not applicable.

Consent for publication
Not applicable.

Competing interests
The authors declare that they have no competing interests.

Author details
[1] Japan Agency for Marine-Earth Science and Technology, 3173-25, Showa-machi, Kanazawa-ku, Yokohama, Kanagawa 236-0001, Japan. [2] Earthquake Research Institute, The University of Tokyo, 1-1-1, Yayoi, Bunkyo-ku, Tokyo 113-0032, Japan. [3] Tokyo University of Marine Science and Technology, 4-5-7, Konan, Minato-ku, Tokyo 108-8477, Japan.

Received: 10 February 2020 Accepted: 19 May 2020
Published online: 27 May 2020

References
Ando M (1975) Source mechanisms and tectonic significance of historical earthquakes along the Nankai trough. Tectonophysics 27:119–140. https://doi.org/10.1016/0040-1951(75)90102-X
Araki E, Saffer DM, Kopf AJ, Wallace LM, Kimura T, Machida Y, Ide S, Davis E, IODP Expedition 365 Shipboard Scientists (2017) Recurring and triggered slow-slip events near the trench at the Nankai Trough subduction megathrust. Science 356:1157–1160. https://doi.org/10.1126/science.aan3120
Bangs NLB, Moore GF, Gulick SPS, Pangborn EM, Tobin HJ, Kuramoto S, Taira A (2009) Broad, weak regions of the Nankai megathrust and implications for shallow coseismic slip. Earth Planet Sci Lett 284:44–49. https://doi.org/10.1016/j.epsl.2009.04.026
Bird P (2003) An updated digital model of plate boundaries. Geochem Geophys Geosyst 4:1027. https://doi.org/10.1029/2001GC000252
Geersen J, Ranero C, Barckhausen U, Reichert C (2015) Subducting seamounts control interplate coupling and seismic rupture in the 2014 Iquique earthquake area. Nat Commun 6:8267. https://doi.org/10.1038/ncomms9267
Ito Y, Obara K (2006) Dynamic deformation of the accretionary prism excites very low frequency earthquakes. Geophys Res Lett 33:L02311. https://doi.org/10.1029/2005GL025270
Ito Y, Obara K, Shiomi K, Sekine S, Hirose H (2007) Slow earthquakes coincident with episodic tremors and slow slip events. Science 315:503–506. https://doi.org/10.1126/science.1134454
Kamei R, Pratt RG, Tsuji T (2012) Waveform tomography imaging of a megasplay fault system in the seismogenic Nankai subduction zone. Earth Planet Sci Lett 317–318:343–353. https://doi.org/10.1016/j.epsl.2011.10.042
Kaneda Y, Kawaguchi K, Araki E, Matsumoto H, Nakamura T, Kamiya S, Ariyoshi K, Hori T, Baba T, Takahashi N (2015) Development and application of an advanced ocean floor network system for megathrust earthquakes and tsunamis. In: Favali P et al (eds) Seafloor observatories. Springer, Heidelberg, pp 643–662. https://doi.org/10.1007/978-3-642-11374-1_252
Kawaguchi K, Kaneko S, Nishida T, Komine T (2015) Construction of the DONET real-time seafloor observatory for earthquakes and tsunami monitoring. In: Favali P et al (eds) Seafloor observatories. Springer, Heidelberg, pp 211–228. https://doi.org/10.1007/978-3-642-11374-1_10
Kimura G, Moore GF, Strasser M, Screaton E, Curewitz D, Streiff C, Tobin H (2011) Spatial and temporal evolution of the megasplay fault in the Nankai Trough. Geochem Geophys Geosyst 12:Q0A008. https://doi.org/10.1029/2010gc003335
Kimura G, Hashimoto Y, Kitamura Y, Yamaguchi A, Koge H (2014) Middle Miocene swift migration of the TTT triple junction and rapid crustal growth in southwest Japan: a review. Tectonics 33:1219–1238. https://doi.org/10.1002/2014TC003531
Kitajima H, Saffer DM (2012) Elevated pore pressure and anomalously low stress in regions of low frequency earthquakes along the Nankai Trough subduction megathrust. Geophys Res Lett 39:L23301. https://doi.org/10.1029/2012GL053793
Kodaira S, Takahashi N, Nakanishi A, Hiura S, Kaneda Y (2000) Subducted seamount imaged in the rupture zone of the 1946 Nankaido earthquake. Science 289:104–106. https://doi.org/10.1126/science.289.5476.104
Kostoglodov V, Singh SK, Santiago JA, Franco SI, Larson KM, Lowry AR, Bilham R (2003) A large silent earthquake in the Guerrero seismic gap, Mexico. Geophys Res Lett 30:1807. https://doi.org/10.1029/2003GL017219
Lin W, Byrne TB, Kinoshita M, McNeill LC, Chang C, Lewis JC, Yamamoto Y, Saffer DM, Moore JC, Wu HT, Tsuji T, Yamada Y, Conin M, Saito S, Ito T, Tobin HJ, Kimura G, Kanagawa K, Ashi J, Underwood MB, Kanamatsu T (2016) Distribution of stress state in the Nankai subduction zone, southwest Japan and a comparison with Japan Trench. Tectonophysics 692:120–130. https://doi.org/10.1016/j.tecto.2015.05.008
Marfurt KJ, Kirlin RL, Farmer SL, Bahorich MS (1998) 3-D seismic attributes using a semblance-based coherence algorithm. Geophysics 63:1150–1165. https://doi.org/10.1190/1.1444415
Miyazaki S, Heki K (2001) Crustal velocity field of southwest Japan: subduction and arc-arc collision. J Geophys Res 106:4305–4326. https://doi.org/10.1029/2000JB900312
Mochizuki K, Yamada T, Shinohara M, Yamanaka Y, Kanazawa T (2008) Weak interplate coupling by seamounts and repeating M ~ 7 earthquakes. Science 321:1194–1197. https://doi.org/10.1126/science.1160250
Moore GF, Bangs NL, Taira A, Kuramoto S, Pangborn E, Tobin HJ (2007) Three-dimensional splay fault geometry and implications for tsunami generation. Science 318:1128–1131. https://doi.org/10.1126/science.1147195
Moore GF, Park JO, Bangs NL, Gulick SP, Tobin HJ, Nakamura Y, Sato S, Tsuji T, Yoro T, Tanaka H, Uraki S, Kido Y, Sanada Y, Kuramoto, S, Taira A (2009) Structural and seismic stratigraphic framework of the NanTroSEIZE Stage 1 transect. In: Proceedings of the Integrated Ocean Drilling Program, Volume 314/315/316. Washington, DC.: Integrated Ocean Drilling Program Management International, Inc. https://doi.org/10.2204/iodp.proc.314315316.102
Nakanishi A, Kodaira S, Miura S, Ito A, Sato T, Park JO, Kido Y, Kaneda Y (2008) Detailed structural image around splay-fault branching in the Nankai subduction seismogenic zone: results from a high-density ocean bottom seismic survey. J Geophys Res 113:B03105. https://doi.org/10.1029/2007JB004974
Nakano M, Hori T, Araki E, Kodaira S, Ide S (2018) Shallow very-low-frequency earthquakes accompany slow slip events in the Nankai subduction zone. Nat Commun 9:984. https://doi.org/10.1038/s41467-018-03431-5

Nishikawa T, Matsuzawa T, Ohta K, Uchida N, Nishimura T, Ide S (2019) The slow earthquake spectrum in the Japan Trench illuminated by the S-net seafloor observatories. Science 365:808–813. https://doi.org/10.1126/science.aax5618

Obana K, Kodaira S (2009) Low-frequency tremors associated with reverse faults in a shallow accretionary prism. Earth Planet Sci Lett 287:168–174. https://doi.org/10.1016/j.epsl.2009.08.005

Obara O, Kato A (2016) Connecting slow earthquakes to huge earthquakes. Science 353(6296):253–257. https://doi.org/10.1126/science.aaf1512

Park JO, Moore GF, Tsuru T, Kodaira S, Kaneda Y (2003) A subducted oceanic ridge influencing the Nankai megathrust earthquake rupture. Earth Planet Sci Lett 217:77–84. https://doi.org/10.1016/S0012-821X(03)00553-3

Park JO, Fujie G, Wijerathne L, Hori T, Kodaira S, Fukao Y, Moore GF, Bangs NL, Kuramoto S, Taira A (2010) A low-velocity zone with weak reflectivity along the Nankai subduction zone. Geology 38:283–286. https://doi.org/10.1130/G30205.1

Rogers G, Dragert H (2003) Episodic tremor and slip on the Cascadia subduction zone: the chatter of silent slip. Science 300:1942–1943. https://doi.org/10.1126/science.1084783

Ruh JB, Sallarès V, Ranero CR, Gerya T (2016) Crustal deformation dynamics and stress evolution during seamount subduction: high-resolution 3-D numerical modeling. J Geophys Res Solid Earth 121:6880–6902. https://doi.org/10.1002/2016JB013250

Sakaguchi A, Chester F, Curewitz D, Fabbri O, Goldsby D, Kimura G, Li CF, Masaki Y, Screaton EJ, Tsutsumi A, Ujiie K, Yamaguchi A (2011) Seismic slip propagation to the updip end of plate boundary subduction interface faults: vitrinite reflectance geothermometry on Integrated Ocean Drilling Program NanTro SEIZE cores. Geology 39:395–398. https://doi.org/10.1130/G31642.1

Seno T, Stein S, Gripp AE (1993) A model for the motion of the Philippine Sea plate consistent with Nuvel-1 and geological data. J Geophys Res 98:17941–17948. https://doi.org/10.1029/93JB00782

Shaddox HR, Schwartz SY (2019) Subducted seamount diverts shallow slow slip to the forearc of the northen Hkurangi subduction zone, New Zealand. Geology 47:415–418. https://doi.org/10.1130/G45810.1

Sheriff RE (2002) Encyclopedic dictionary of applied geophysics. Society of Exploration Geophysicist, Tulsa. https://doi.org/10.1190/1.9781560802969

Sherwood JWC, Sherwood K, Tieman H, Schileicher K (2009) 3D beam prestack depth migration with examples from around the world. Lead Edge 28:1120–1127. https://doi.org/10.1190/1.3236382

Shiraishi K, Moore GF, Yamada Y, Kinoshita M, Sanada Y, Kimura G (2019a) Seismogenic zone structures revealed by improved 3-D seismic images in the Nankai Trough off Kumano. Geochem Geophys Geosyst 20:2252–2271. https://doi.org/10.1029/2018GC008173

Shiraishi K, Yamada Y, Nibe T (2019b) Thermogenic petroleum potential of the Nankai subduction zone, offshore SW Japan. J Pet Geol 42:417–434. https://doi.org/10.1111/jpg.12744

Strasser M, Moore GF, Kimura G, Kitamura Y, Kopf AJ, Lallemant S, Park JO, Screaton EJ, Su X, Underwood MB, Zhao X (2009) Origin and evolution of a splay fault in the Nankai accretionary wedge. Nat Geosci 2:648–652. https://doi.org/10.1038/NGEO609

Sugioka H, Okamoto T, Nakamura T, Ishihara Y, Ito A, Obana K, Kinoshita M, Nakahigashi K, Shinohara M, Fukao Y (2012) Tsunamigenic potential of the shallow subduction plate boundary inferred from slow seismic slip. Nat Geosci 5:414–418. https://doi.org/10.1038/ngeo1466

Sun T, Saffer D, Elis S (2020) Mechanical and hydrological effects of seamount subduction on megathrust stress and slip. Nat Geosci 13:249–255. https://doi.org/10.1038/s41561-020-0542-0

Taira A (2001) Tectonic evolution of the Japanese Island arc system. Annu Rev Earth Planet Sci 29:109–134. https://doi.org/10.1146/annurev.earth.29.1.109

Takemura S, Matsuzawa T, Noda A, Tonegawa T, Asano Y, Kimura T, Shiomi K (2019) Structural characteristics of the Nankai Trough shallow plate boundary inferred from shallow very low frequency earthquakes. Geophys Res Lett 46:4192–4201. https://doi.org/10.1029/2019GL082448

Todd EK, Schwartz SY, Mochizuki K, Wallace LM, Sheehan AF, Webb SC, William CA, Nakai J, Yarce J, Fry B, Henrys S, Ito Y (2018) Earthquakes and tremor linked to semount subduction during shallow slow slip at the Hikurangi Margin, New Zealand. J Geophys Res Solid Earth 123:6269–6783. https://doi.org/10.1029/2018JB016136

Toh A, Obana K, Araki E (2018) Distribution of very low frequency earthquakes in the Nankai accretionary prism influenced by a subducting-ridge. Earth Planet Sci Lett 482:342–356. https://doi.org/10.1016/j.epsl.2017.10.062

Tonegawa T, Araki E, Kimura T, Nakamura T, Nakano M, Suzuki K (2018) Sporadic low-velocity volumes spatially correlate with shallow very low frequency earthquake clusters. Nat Commun 8:2048. https://doi.org/10.1038/s41467-017-02276-8

Tsuji T, Park JO, Moore G, Kodaira S, Fukao Y, Kuramoto S, Bangs N (2009) Intraoceanic thrusts in the Nankai Trough off the Kii Peninsula: implications for intraplate earthquakes. Geophys Res Lett 36:L06303. https://doi.org/10.1029/2008GL036974

Tsuji T, Kodaira S, Ashi J, Park JO (2013) Widely distributed thrust and strike-slip faults within subducting oceanic crust in the Nankai Trough off the Kii Peninsula, Japan. Tectonophysics 600:52–62. https://doi.org/10.1016/j.tecto.2013.03.014

Tsuji T, Kamei R, Pratt RG (2014) Pore pressure distribution of a mega-splay fault system in the Nankai Trough subduction zone: insight into up-dip extent of the seismogenic zone. Earth Planet Sci Lett 396:165–178. https://doi.org/10.1016/j.epsl.2014.04.011

Uunderwood MB, Saito S, Kubo Y, the Expedition 322 Scientists (2010) Expedition 322 summary. In: Saito S, Underwood MB, Kubo Y, the Expedition 322 Scientists, Proceedings of the Integrated Ocean Drilling Program, Volume 322. Integrated Ocean Drilling Program Management International, Inc. Tokyo. https://doi.org/10.2204/iodp.proc.322.101.2010

Wallace LM, Beavan J (2010) Diverse slow slip behavior at the Hikurangi subduction margin, New Zealand. J Geophys Res 115:B12402. https://doi.org/10.1029/2010JB007717

Wallace LM, Webb SC, Ito Y, Mochizuki K, Hino R, Henrys S, Schwartz SY, Sheehan AF (2016) Slow slip near the trench at the Hikurangi subduction zone, New Zealand. Science 352:701–704. https://doi.org/10.1126/science.aaf2349

Wang K, Bilek SL (2011) Do subducting seamounts generate or stop large earthquakes? Geology 39(9):819–822. https://doi.org/10.1130/G31856.1

Wang K, Bilek SL (2016) Invited review paper: fault creep caused by subduction of rough seafloor relief. Tectonophysics 610:1–24. https://doi.org/10.1016/j.tecto.2013.11.024

Yamada Y, Masui R, Tsuji T (2013) Characteristics of a tsunamigenic megasplay fault in the Nankai Trough. Geophys Res Lett 40:4594–4598. https://doi.org/10.1002/grl.50888

Yamashita Y, Yakiwara H, Asano Y, Shimizu H, Uchida K, Hirano S, Umakoshi K, Miyamachi H, Nakamoto M, Fukui M, Kamizono M, Kanehara H, Yamada T, Shinohara M, Obara K (2015) Migrating tremor off southern Kyushu as evidence for slow slip of a shallow subduction interface. Science 348:676–679. https://doi.org/10.1126/science.aaa4242

Publisher's Note